IEEE Access
Multidisciplinary | Rapid Review | Open Access Journal

Received January 26, 2020, accepted February 3, 2020, date of publication February 11, 2020, date of current version February 25, 2020.

Digital Object Identifier 10.1109/ACCESS.2020.2973191

Deception Jamming Against Doppler Beam Sharpening Radars

GARETH FRAZER[1], ALESSIO BALLERI[1], AND GEORGE JACOB[2]
[1]Centre for Electronic Warfare, Information and Cyber, Defence Academy of the UK, Cranfield University, Shrivenham SN6 8LA, U.K.
[2]Defence Science and Technology Laboratory, Salisbury SP4 0JQ, U.K.

Corresponding author: Alessio Balleri (a.balleri@cranfield.ac.uk)

This work was supported in part by the Defence Science and Technology Laboratory (Dstl), and the Engineering and Physical Sciences Research Council (EPSRC).

ABSTRACT Missile seekers are becoming increasingly more capable of using Doppler Beam Sharpening (DBS) modes as part of the homing cycle, which requires new countermeasures against this mode. One type of countermeasure, is to create false targets within the seeker DBS image. This paper proposes a jamming technique to generate false targets at a precise location within a seeker DBS image, by both delaying and adding a Doppler shift to received waveforms. The effects of tracking errors on the position of the false target are analysed, both analytically and with simulations and used to assess the practical implementation of the jamming scheme. An experimental DBS system was built to test the effectiveness of the jamming scheme against a platform moving in steps and assess errors caused by incorrectly estimating the seeker trajectory.

INDEX TERMS Anti-ship missile, DBS, false targets.

I. INTRODUCTION

Doppler Beam Sharpening (DBS) is a technique that uses the changing Doppler frequency caused by relative motion between a platform and a target, to synthetically narrow the main beam of the antenna and generate an image. It is a type of imaging radar, often used for ground mapping and clutter discrimination [1]. Whilst it is quite an old technique (dating back to the 1950's), it is now being used in missiles [2], naval radars [3] and in the automotive industry [4], [5]. Missile seekers benefit from using DBS, as it provides a crude imaging capability by improving azimuth resolution without being computationally expensive, like Synthetic Aperture Radars (SAR). DBS images are typically much faster to obtain than SAR images and easier to analyse, whereas SAR tends to have a vastly superior azimuth resolution and focus. As a generic example, DBS can be performed with a dwell time in the order of tens of milliseconds, whereas SAR is in the order of whole seconds [6].

Countermeasures against RF missile seekers have attracted the interest of the Electronic Warfare community for decades. For example, techniques against conventional monopulse radars have been intensely studied. A monopulse radar is a widely used tracking radar, employed by many modern missile seekers and there are several methods to jam this type of radar. One such method is the use of noise jamming. Paik et al [7]–[9] have undertaken several studies into noise jamming monopulse radars. They have investigated conditions in which 'break-lock' of phased locked loops (PLL) in the monopulse occurs when tracking a target.

Another method is to use deception jamming and Neri [10] summarises a few methods of anti-monopulse deception jamming techniques, such as cross-polarisation, cross-eye jamming and the use of decoys. Cross-Eye Jamming (CEJ) aims to create 'worst-case' angular errors in monopulse radars due to glint [11]. The problem with cross-eye jamming is that it requires highly accurate estimation and replication of the seeker waveforms. Falk [12] discusses the principles of cross-eye jamming and explains how scattering of the jamming waveform by ocean waves can severely affect the performance of the jammer. A method of practically implementing cross-eye jamming is retrodirective cross-eye jamming, which is demonstrated in [13] and an extended analysis of retrodirective cross-eye jamming is described in [14]. A derivation of the cross-eye gain in the presence of skin-returns is presented in [15].

In order for cross-eye jamming to be implemented successfully, high fidelity copies of the waveform from the victim radar need to be obtained. The ability to create high fidelity copies of waveforms and modify them comes from

The associate editor coordinating the review of this manuscript and approving it for publication was Davide Comite.

the use of Digital Radio Frequency Memory (DRFM) systems. A DRFM can store and modify waveforms using high-speed sampling and digital memory [16]. The DRFM enables phase coherency, which enables coherent radar modes to be jammed such as by creating false targets in SAR images. A brief overview of using a DRFM to create false targets in SAR images is found in [17]. There has been some active research for creating false targets in SAR images. The work in [18] investigated how to create false targets in a SAR image by modulating the received waveform for a generic scenario.

In addition to investigating narrow and broadband noise jamming (which is beyond the scope of this paper), the research in [19] used a varying time delay method to create false targets in a SAR image. Using this method in practice is difficult as it requires extremely precise timings in hardware. A method to create false targets in a SAR image by modulating the received signal is shown for missile-borne SAR in [20] and space-borne SAR in [21]. Both methods require knowledge of the platform trajectory, as well as the ability to coherently modify the received waveform.

Instead of broadband or narrowband jamming, which requires higher jamming power due to the processing gains of coherent radars, another method is to use Doppler or 'phase noise' jamming. The research in [22] presents this idea. Here, the jammer receives the seeker waveform and then multiplies that waveform by video noise where the phase is randomly distributed. The effect of this jamming is to create a distinct noise band in the range bins (corresponding to the range-resolution of the pulse), which spreads across all of the Doppler bins.

A similar effect is observed in [23] where the authors propose the idea of jittering the jammer hold-on time and multiplying the phase of the received waveform by a noise waveform. They also propose sampling only part of the received waveform so the pulse width is less than the victim radar waveform. This enables the jammer to transmit more jittered pulses within a single PRI, to create a distinct noise band at desired range and Doppler bands. Another method of achieving a similar result is presented in [24]. Here the authors propose using repeat jamming with a random delay against a SAR GMTI (Ground Moving-Target Indication) system.

Whilst not directly related to this paper, there is also some research in jamming bistatic and multistatic SAR systems. In [25], the authors propose transmitting a randomly jittered copy of the received waveform from outside the scene area to mask the presence of targets in the scene. This requires the jammer receiver to be inside the scene area and the employment of a DRFM to store copies of the victim radar waveforms. In [26], the authors propose jamming a bistatic Inverse Synthetic Aperture Radar (ISAR) system by undersampling the waveform of the victim radar in a sub-Nyquist manner. The jammer receives a scattered echo from a moving target and then transmits the undersampled jamming waveform at the moving target in order for the jamming waveform to be scattered towards the victim receiver. This form of deception jamming aims to create multiple false targets with the number of false targets being a function of the undersampling rate used. The sub-Nyquist method to create multiple false targets is also used in [27] against an ISAR system which uses Compressive Sensing (CS).

There has been some unclassified research into optimising the trajectory of a missile specifically to perform DBS which is detailed in [28], [29] and [30]. In order for a jammer to create a false target at a desired location within the seeker DBS image, the jammer must know that the seeker is using the DBS mode. As the signal processing for DBS is similar to that of a pulse-Doppler radar, it is difficult to know when the seeker is performing DBS. Detecting when the seeker would be performing DBS is beyond the scope of this paper, but the optimised trajectories give a potential method of detecting when a seeker is using DBS.

There is very little literature on jamming DBS modes, but previous work in [31] introduced the concept of creating false targets in DBS images of a missile seeker using a varying time delay method. For this method, the jammer receives the incoming waveform and delays it before re-transmitting. If the jammer delay time varies on a pulse per pulse basis, a synthetic phase history can be created to place a false target at a desired location.

Several jamming methods against conventional monopulse radars and imaging radars such as SAR and ISAR have been discussed so far. However, there is very little, if any, existing literature that details how to create a false target at a specific location within a DBS image. Nor does any of the literature explain how positional errors in the false target are induced by incorrectly estimating the platform trajectory. Previous work in [32] introduced the jamming technique proposed in this paper, but it did not provide a rigorous mathematical detail of the technique, analyse errors caused by incorrect seeker trajectory estimation, or use the experimental DBS system used in this paper.

The research in this paper proposes a jamming technique to generate false targets at a precise location within a seeker DBS image, by both delaying and adding a Doppler shift to received waveforms. The effects of tracking errors on the position of the false target are analysed, both analytically and with simulations and used to assess the practical implementation of the jamming scheme. An experimental DBS system was built to test the effectiveness of the jamming scheme against a platform moving in steps and assess errors caused by incorrectly estimating the seeker trajectory.

II. GEOMETRY AND SIGNAL MODEL

Let us consider a missile seeker transmitting a signal

$$s_T(t) = s(t)e^{i2\pi f_c t} \tag{1}$$

flying along the x-axis of a 2D Cartesian coordinate system with dynamics

$$x(t) = Vt \tag{2}$$

and constant velocity V.

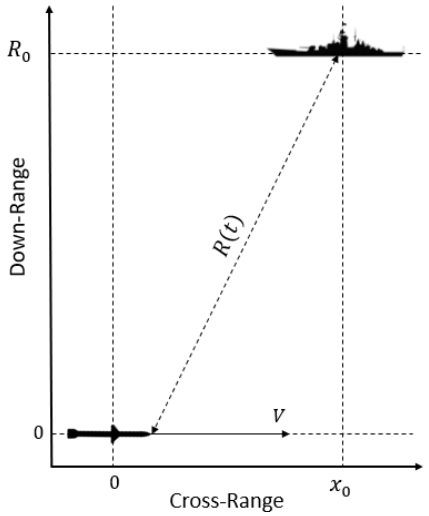

FIGURE 1. Missile reference frame.

The signal reflected from a target located at a slant range R_0 and cross-range x_0, as shown in Figure 1, can be expressed as

$$s_R(t) = \gamma_R\, s(t - \tau(t)) e^{-i2\pi f_c \tau(t)} e^{i2\pi f_c t} \tag{3}$$

where

$$\tau(t) = \frac{2R(t)}{c} \tag{4}$$

is the echo time delay and

$$R(t) = \sqrt{(x_0 - Vt)^2 + {R_0}^2} \tag{5}$$

is the instantaneous target distance from the missile. For $R_0 \gg x_0$ and $t \approx 0$

$$R(t) \simeq R_0 \sqrt{1 - \frac{2Vtx_0}{{R_0}^2}} \tag{6}$$

which after a first order Taylor approximation about $t = 0$ leads to

$$R(t) = R_0 - \frac{Vx_0}{R_0} t \tag{7}$$

and

$$\tau(t) = \frac{2R_0}{c} - \frac{2Vx_0}{cR_0} t \tag{8}$$

Finally, the signal received by the seeker after IQ demodulation can be expressed as

$$s_R(t) = \gamma_R\, s(t - \tau(t)) e^{-i\frac{4\pi}{\lambda}R_0} e^{i2\pi \frac{2Vx_0}{\lambda R_0} t} \tag{9}$$

which after the narrowband approximation [33] becomes

$$s_R(t) = \gamma_R\, s(t - \frac{2R_0}{c}) e^{-i\frac{4\pi}{\lambda}R_0} e^{i2\pi \frac{2Vx_0}{\lambda R_0} t} \tag{10}$$

where γ_R is the two-way attenuation factor. Eq. (10) shows that the received signal is a delayed copy of the transmitted signal shifted in Doppler of $f_D = \frac{2Vx_0}{\lambda R_0}$. DBS measures the Doppler shift and obtains an estimate of the slant range to find the cross-range coordinate of the target.

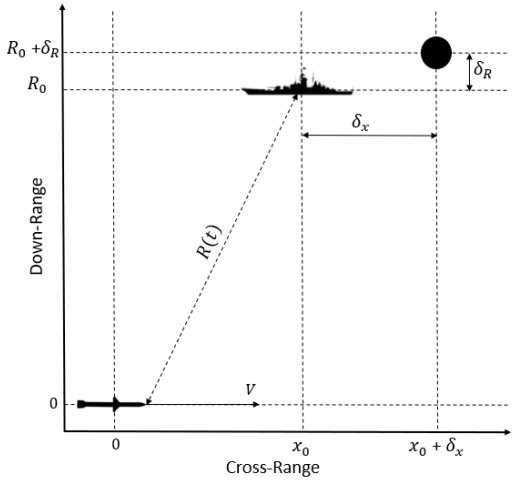

FIGURE 2. Missile reference frame with jammer.

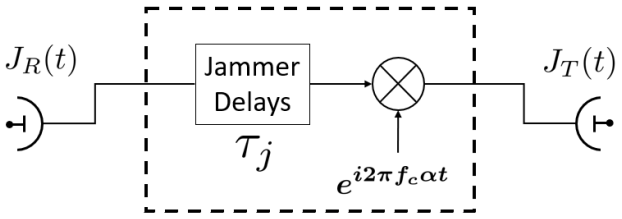

FIGURE 3. Jamming block diagram.

III. JAMMING THEORY AND METHOD

A. THEORY

This section develops the theory used to create a false target at a specific location within the seeker DBS image, as well as detailing how the position of the false target will change, if incorrect seeker trajectory parameters (e.g. velocity or range) are used by the jammer.

The signal model presented in Section II is now extended to the case of a target capable of intercepting the signal transmitted by the RF seeker to re-transmit a suitably modified jamming version and place a false target in a desired location of coordinates $(x_0 + \delta_x, R_0 + \delta_R)$. Figure 2 details the scenario with the position of the intended false target.

In this paper, the jamming scheme outlined in Figure 3 is proposed for which the jammer can generate false targets by applying a time delay τ_j and a Doppler shift $f_J = \alpha f_D$ to the intercepted waveform. The goal of the jammer is to calculate τ_j and the parameter α, based on the received signal, to place the false target at the desired miss-distance in downrange and cross-range.

Let the transmitted signal $s_T(t)$ from the seeker be the same of Eq. (1) where $s(t)$ is an arbitrary complex envelope of the waveform. Whilst propagating towards the jammer, $s_T(t)$ will experience a time delay

$$\tau(t) = \frac{R(t - \tau(t))}{c} = \frac{R_0}{c} + \frac{\beta}{c}[t - \tau(t)] \tag{11}$$

with

$$\beta = -\frac{Vx_0}{R_0} \tag{12}$$

which after a simple algebraic manipulation can be expressed as

$$\tau(t) = \frac{R_0}{(c+\beta)} + \frac{\beta t}{(c+\beta)} \tag{13}$$

The signal received by the jammer is therefore

$$j_R(t) = \gamma\, s_T\Big(t - \frac{R_0}{(c+\beta)} - \frac{\beta t}{(c+\beta)}\Big) \tag{14}$$

where γ is a one way attenuation factor. The jammer would then delay $j_R(t)$ by τ_j, to give an additive range component, and induce a Doppler shift to then transmit

$$j_T(t) = \gamma_J\, s_T\left(\frac{c}{(c+\beta)}t - \frac{c\tau_j}{(c+\beta)} - \frac{R_0}{(c+\beta)}\right) \times \exp(i2\pi f_c \alpha t) \tag{15}$$

where γ_J is the jammer amplitude factor. The second leg of propagation back towards the seeker has the delay of

$$\tau'(t) = \frac{R(t)}{c} = \frac{R_0}{c} + \frac{\beta t}{c} \tag{16}$$

This gives the resulting jamming signal to be

$$s_R(t) = \gamma_R\, s_T\left(\frac{c}{(c+\beta)}[t - \tau'(t)] - \frac{c\tau_j + R_0}{(c+\beta)}\right) \times \exp\big(i2\pi f_c \alpha[t - \tau'(t]\big) \tag{17}$$

which, after replacing the value of $\tau'(t)$ in Eq. (16), can be written as

$$s_R(t) = \gamma_R\, s_T\left(\frac{c-\beta}{(c+\beta)}t - \frac{c}{(c+\beta)}\left[\frac{2R_0}{c} + \tau_j\right]\right) \times \exp\big(i2\pi f_c \alpha \frac{c-\beta}{c}t\big) \exp\big(-i2\pi f_c \alpha \frac{R_0}{c}\big) \tag{18}$$

After replacing the expression of s_T(t) in Eq. (1), the signal received at the seeker can be expressed as

$$\begin{aligned} s_R(t) &= \gamma_R\, s\left(\frac{c-\beta}{c+\beta}t - \frac{c}{(c+\beta)}\left[\frac{2R_0}{c} + \tau_j\right]\right) \\ &\times \exp\left(i2\pi f_c \frac{c-\beta}{c+\beta}t\right) \exp\left(-i2\pi f_c \frac{c}{(c+\beta)}\left[\frac{2R_0}{c} + \tau_j\right]\right) \\ &\times \exp\big(i2\pi f_c \alpha \frac{c-\beta}{c}t\big) \exp\big(-i2\pi f_c \alpha \frac{R_0}{c}\big) \end{aligned} \tag{19}$$

which after down-conversion becomes

$$\begin{aligned} s_R(t) &= \gamma_R\, s\left(\frac{c-\beta}{c+\beta}t - \frac{c}{(c+\beta)}\left[\frac{2R_0}{c} + \tau_j\right]\right) \\ &\times \exp\left(-i2\pi f_c \frac{2\beta}{c+\beta}t\right) \exp\left(-i2\pi f_c \frac{c}{(c+\beta)}\left[\frac{2R_0}{c} + \tau_j\right]\right) \\ &\times \exp\big(i2\pi f_c \alpha \frac{c-\beta}{c}t\big) \exp\big(-i2\pi f_c \alpha \frac{R_0}{c}\big) \end{aligned} \tag{20}$$

When $\beta \ll c$, the terms $\frac{c}{c+\beta} \simeq 1$, $\frac{2\beta}{c+\beta} \simeq \frac{2\beta}{c}$ and $\frac{c-\beta}{c} \simeq 1$, and after the narrowband approximation [33] the final waveform at the seeker becomes

$$s_R(t) = \hat{\gamma}_R\, s\left(t - \frac{2R_0}{c} - \tau_j\right) \times \exp\left(-i2\pi f_c \frac{2\beta}{c}t\right) \exp\left(i2\pi f_c \alpha t\right) \tag{21}$$

where all constant phase terms have been included in the parameter $\hat{\gamma}_R$. From Eq. (10), an ideal target located at $(x_0 + \delta_x, R_0 + \delta_R)$ would generate an echo signal

$$s_R(t) = \gamma_R\, s\left(t - \frac{2(R_0+\delta_R)}{c}\right) \times \exp\left(-i4\pi \frac{(R_0+\delta_R)}{c}\right) \exp\left(i2\pi \frac{2V(x_0+\delta_x)t}{\lambda(R_0+\delta_R)}\right) \tag{22}$$

In order for the jammer to create the perfect false target, the value of τ_j and α must be such that the total time delay and Doppler shift at the seeker in Eq. (21) are the same as that for in Eq. (22).

If

$$\beta_J = -\frac{V(x_0+\delta_x)}{(R_0+\delta_R)} \tag{23}$$

then α can be calculated by imposing the Doppler equality

$$-f_c \frac{2\beta}{c} + f_c \alpha = -f_c \frac{2\beta_j}{c} \tag{24}$$

which leads to the final result

$$\alpha = \frac{2\beta}{c} - \frac{2\beta_J}{c} = \frac{2V(x_0+\delta_x)}{c(R_0+\delta_R)} - \frac{2Vx_0}{cR_0} \tag{25}$$

Similarly, it is straightforward to show that

$$\tau_j = \frac{2\delta_r}{c} \tag{26}$$

These results show that in order to generate a false target in the desired cross-range location, the jammer must create a synthetic phase history to mimic the phase history a target would have, if it was at that location. This requires the jammer to have perfect knowledge of its position with respect to the seeker. It is finally important to observe that the analytical results presented in this section are general and apply to any type of waveform design $s(t)$.

B. PULSED DBS THEORY

Consider a pulsed waveform,

$$s(t) = \sum_{m=0}^{M-1} x(t - mPRI) \tag{27}$$

consisting of M pulses of duration τ. Following the result obtained in Eq. (21), the signal received by the seeker would be

$$s_R(t) = \hat{\gamma}_R \sum_{m=0}^{M-1} x\left(t - mPRI - \frac{2R_0}{c} - \tau_j\right) \times \exp\left(-i2\pi f_c \frac{2\beta}{c}t\right) \exp\left(i2\pi f_c \alpha t\right) \tag{28}$$

where *PRI* is the Pulse Repetition Interval. If the time domain is sampled in a fast-time, slow-time form with $t = t_1 + kPRI$ and $0 < t_1 < PRI$, the received signal can be expressed as

$$s_R(t_1, k) = \hat{\gamma}_R \sum_{m=0}^{M-1} x\left(t_1 - (m-k)PRI - \frac{2R_0}{c} - \tau_j\right) \times \exp\left(-i2\pi f_c \frac{2\beta}{c} t_1\right) \exp\left(-i2\pi f_c \frac{2\beta}{c} kPRI\right) \times \exp\left(i2\pi f_c \alpha t_1\right) \exp\left(i2\pi f_c \alpha kPRI\right) \quad (29)$$

For a fixed range bin, the phase terms containing t_1 will be constant from pulse to pulse. This therefore means they can be placed into the term $\hat{\gamma}_R$, which contains the other constant phase terms. It is straightforward to show that when the pulse width is less than the PRI ($\tau <$ PRI), the received pulse train at the seeker is

$$s_R(t_1, k) = \hat{\gamma}_R\, x\left(t_1 - \frac{2R_0}{c} - \tau_j\right) \exp\left(-i2\pi f_c \frac{2\beta}{c} kPRI\right) \exp\left(i2\pi f_c \alpha kPRI\right) \quad (30)$$

Eq.(30) shows that for a pulsed waveform, introducing a false target in a fixed range bin is equivalent to introducing an incremental phase shift from pulse to pulse. This will be exploited for the experimental demonstration of the results where a 'stop and go' method is employed to carry out measurements without the use of a DFRM.

C. ERRONEOUS TRAJECTORY ESTIMATION

The algorithm proposed in this paper relies on estimates of the position and velocity of the missile which are provided by a tracking radar co-located with the jammer. The tracking radar may have bias in the position and velocity estimates of the missile. The tracking radar bias can be evaluated at calibration stage and compensated for before passing the information to the jammer. However, in cases where the bias cannot be eliminated, the jammer will use incorrect values of x_0, R_0 and V. A false target will still be created, but not at the desired location. The performance of the false target position is now presented. Each variable in Eq. (25) can be incorrectly estimated by varying amounts. Incorporating these errors into in Eq. (25) gives:

$$\alpha_\epsilon = \frac{2}{c}\left[\frac{V_\epsilon V(x_\epsilon x_0 + \delta_x)}{(R_\epsilon R_0 + \delta_R)} - \frac{V_\epsilon V x_\epsilon x_0}{R_\epsilon R_0}\right] \quad (31)$$

The scalar variables x_ϵ, R_ϵ and V_ϵ are the numerical ratio between the estimated value of the variable and the true value for cross-range, downrange and velocity respectively. For example, if the true velocity of the missile is 300m/s but the jammer estimates it to be 360m/s, then $V_\epsilon = \frac{V_j}{V} = 1.2$. Incorporating this into the signal in Eq. (21), the resultant signal would be:

$$s_R(t) = \hat{\gamma}_R\, s\left(t - \frac{2R_0}{c} - \tau_j\right) \exp\left(-i2\pi f_c \frac{2\beta t}{c}\right) \times \exp\left(i2\pi f_c t \frac{2}{c}\left[\frac{V_\epsilon V(x_\epsilon x_0 + \delta_x)}{(R_\epsilon R_0 + \delta_R)} - \frac{V_\epsilon V x_\epsilon x_0}{R_\epsilon R_0}\right]\right) \quad (32)$$

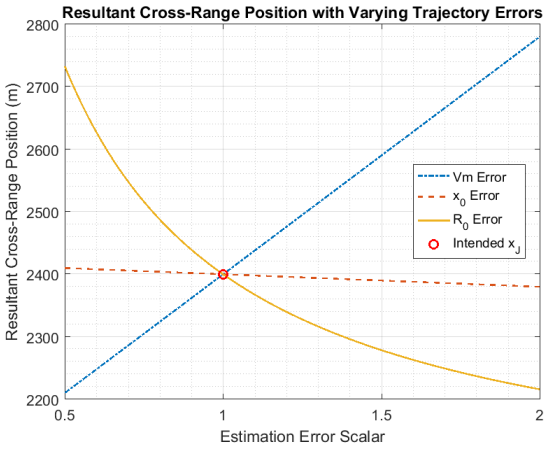

FIGURE 4. Resultant cross-range position with varying errors when $V = 272$ m/s, $R_0 = 20$km, $x_0 = 2$km and $\delta_x = 400$m.

with instantaneous frequency

$$f_d = \frac{2}{\lambda}\left(\frac{V_\epsilon V(x_\epsilon x_0 + \delta_x)}{(R_\epsilon R_0 + \delta_R)} - \frac{V_\epsilon V x_\epsilon x_0}{R_\epsilon R_0} + \frac{V x_0}{R_0}\right) \quad (33)$$

If there were no errors in the missile trajectory, Eq. (32) would simplify to Eq. (22). To obtain the cross range position of the target, the seeker would then invert the Doppler equation to map for the cross-range position at each range bin. Therefore the cross-range position for the false target will be

$$\hat{x} = (R_0 + \delta_R)\left(\frac{V_\epsilon(x_\epsilon x_0 + \delta_x)}{(R_\epsilon R_0 + \delta_R)} - \frac{V_\epsilon x_\epsilon x_0}{R_\epsilon R_0} + \frac{x_0}{R_0}\right) \quad (34)$$

This equation predicts how the position of the false target will change with erroneous trajectory estimation for a linearly moving missile.

Figure 4 shows how the cross-range position of the false target will shift when x_ϵ, R_ϵ and $V\epsilon$ from Eq. (31) are systematically varied for a seeker, where $V = 272$ m/s, $R_0 = 20$km, $x_0 = 2$km and $\delta_x = 400$m. For example, the plot for the velocity error uses

$$\alpha_\epsilon = \frac{2}{c}\left[\frac{V_\epsilon V(x_0 + \delta_x)}{(R_0 + \delta_R)} - \frac{V_\epsilon V x_0}{R_0}\right] \quad (35)$$

Figure 4 shows that an erroneous velocity estimation will yield the largest errors in the position of the false target. The purpose of jamming a missile or tracking radar is to avoid being hit by the missile or tracked by the enemy. Therefore, it is likely to be more desirable to have a false target at a location further away than intended, than closer, to avoid being hit. Using this principle, Figure 4 shows it is better to underestimate the cross-range and down-range variables and overestimate the velocity magnitude variable. This is a general result, which will hold when $R_0 \gg x_0$.

In order for the jammer to correctly modify the waveforms, data from a tracking radar will need to be fed into the jamming system. This would likely be from the on-board surveillance and tracking radars that military ships will use.

TABLE 1. Generic tracking radar parameters.

Variable	Symbol	Value
Carrier Frequency	f_c	3GHz
Bandwidth	B	100MHz
Pulse Width	T	10μs
Pulse Repetition Frequency	PRF	20kHz
3dB Horizontal Beamwidth	θ	2°
Dwell Time	Δt	1ms
Assumed SNR	SNR	3dB
Range	R	20km
Azimuth Error	Δ_x	415.27m
Range Error	Δ_R	1.78m
Doppler Error	Δ_{fd}	59.50Hz

To better understand the size and scale of the errors, parameters for a generic tracking radar have been used to calculate the expected magnitude of measurement errors (for a single pulse) that a radar could theoretically have. A tracker could potentially improve on these errors, so the equations are used to gain an understanding of the magnitude of the respective errors, in a general case. These errors occur when taking various measurements about a target in the presence of Gaussian white noise. General equations for measurement errors for azimuth, range and Doppler are listed as follows [34]:

$$\Delta_x = \frac{2Rsin\left(\frac{\theta_{3dB}}{2}\right)}{\sqrt{2SNR}} \tag{36}$$

$$\Delta_R = \frac{c}{2B\sqrt{2SNR}} \tag{37}$$

$$\Delta_{fd} = \frac{\lambda}{\Delta t\sqrt{2SNR}} \tag{38}$$

Using the parameters in Table 1 and Eq. (36), (37) and (38), it can be seen that the largest error of the three measurements is that for the cross-range estimate, especially at larger ranges. With instantaneous bandwidths in the order of 100s of MHz, the range errors induced by poor a SNR are small (less than the resolution cell) and almost negligble when the range component is in the order of several kilometres or larger. Whilst the biggest effect on the position of the false target is from the velocity estimation, the expected errors in the Doppler measurement result in the error scalar, $V\epsilon$, potentially being in the order of 1.02 for a missile travelling at 270m/s.

Whilst a tracking radar would improve on these measurement errors, in a contested battlespace, the on-board tracking radar could itself be victim of jamming. This means that the tracking errors may therefore be larger than the theoretical measuring errors and similar to that of Figure 4.

IV. PRACTICALLY MODIFYING A WAVEFORM

In order to test the theory developed in this paper and demonstrate the practical implementation of it, real measurements were taken in a laboratory. The aim of the measurements was twofold; to show that the developed theory is correct and false targets appear in the correct location, as well as to show that the positions of the false target change accordingly, when various parameters of the seeker trajectory are erroneously estimated. The aims of the experiment were met using physical

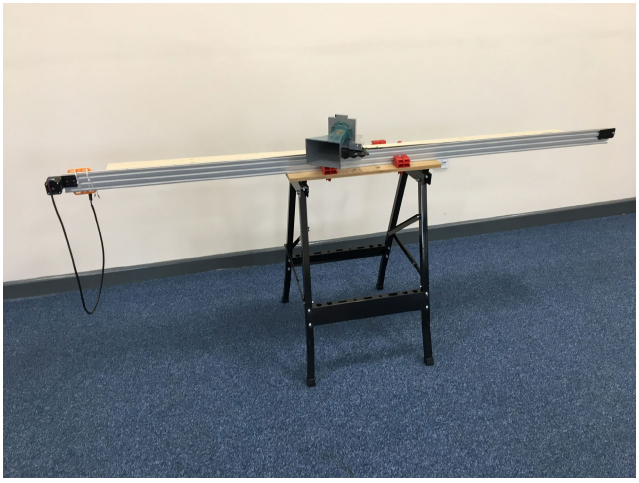

FIGURE 5. Experimental DBS rail.

antenna movement by sliding an antenna across an aperture with respect to a stationary target. The movement was carried out in steps and was used to simulate the linear motion of a missile to test the developed theory.

To do this, a linear belt driven rail was constructed to slide an antenna across an aperture to simulate the seeker trajectory as shown in Figure 5. The rail used is 2m long and is driven by a 'NEMA 17' stepper motor. The motor used had 0.9° resolution with 400 steps per 360° revolution. The breakout board used to interface the Arduino to the stepper motor was an A4988 'StepStick' driver board.

To reduce the complexity of the measurements, a 'stop and go' method was used between pulses, instead of continuously moving the antenna and transmitting. Using this method removed the requirement for instantaneous processing of the transmitted and received waveforms as well as removing the requirement to move the antenna at high speeds. The 'stop and go' method also enabled the simulation of higher velocities or varying PRIs as the antenna can be moved according to the distance the seeker would travel between PRIs. For example, if the PRF is 10kHz and the missile speed 300m/s, the antenna can be moved 3mm between each transmitted pulse. Therefore by controlling the distance moved by the antenna between pulses and assuming a fixed PRF, the speed can be simulated as the Doppler shifts are not observed in fast time, but in slow time between pulses. The 'stop and go' method has been used solely for the scope of demonstrating the jamming technique in the laboratory. As shown in Eq. (22), a higher velocity or varying PRF does not affect the analytical performance of the proposed solution as long as the narrowband approximation in Eq. (21) holds (which is commonly the case for the velocities of the missiles under consideration in this research). From Eq. (30) and for a fixed range bin, the Doppler shift can be induced with respect to slow-time (kPRI) and not fast time. As shown in Figure 6, the range bin will be fixed for the experiment, enabling the 'stop and go' method to be used.

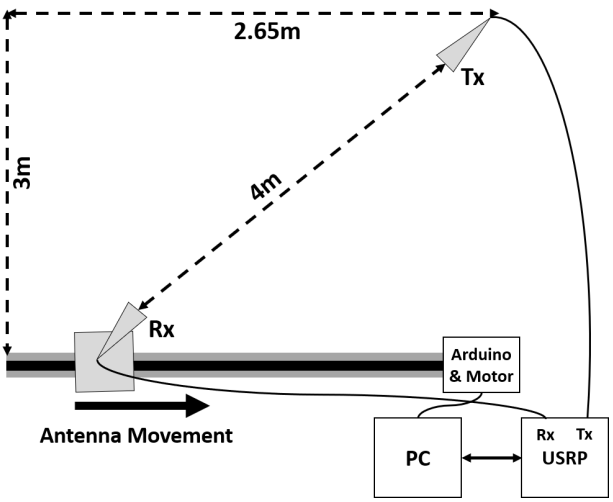

FIGURE 6. Experimental layout.

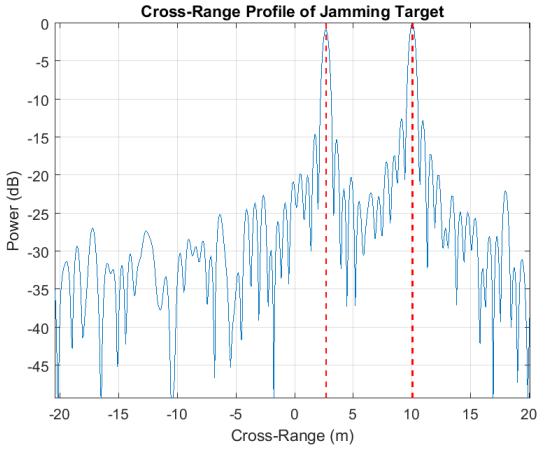

FIGURE 7. Cross-range profile of of 'Echo' and false target when $\tau_J = 0$ and $\delta_x = 7.35$m.

TABLE 2. USRP variables.

Variable	Symbol	Value
Carrier Frequency	f_c	5GHz
Bandwidth	B	30MHz
Pulse Width	τ	$10\mu s$
Sampling Rate	F_s	80MHz
Assumed Missile Velocity	V	60m/s
Pulse Repetition Interval	PRI	$50\mu s$
Number of Pulses	M	128

The accuracy of the rail movement between pulses was tested and it was found that the rail had an average deviation of 0.1mm and a standard deviation of 0.13mm. For a carrier frequency of 5GHz with a wavelength of 60mm, these errors mean that the movement errors are 0.16% of the wavelength and therefore not significant.

For the measurements, two pyramidal horn antennas were used as shown in Figure 6. The measurements were completed in the far-field region of the antennas. No beam steering was used (mechanically or electronically) during the measurement, but the receiving antenna was kept inside the main beam of the transmitter for all of the transmitted pulses. The horizontal beamwidth used is calculated by [35]:

$$\theta_h = \frac{51\lambda}{W} = \frac{51 \times 0.06}{0.09} = 34^\circ \tag{39}$$

where W is the width of the antenna at the flared end. This means at a range of 4m, the cross-range resolution of the real beam is $2R \sin\left(\frac{\theta_h}{2}\right)$ and therefore ≈ 2.34m.

The waveforms were generated with a Universal Software Radio Peripheral (USRP) made by National Instruments (NI-2943R). LabVIEW was used to control both the USRP and the Arduino and Matlab was embedded into the LabView program to design the waveforms. Table 2 shows the signal variables for the measurements and Figure 6 shows the geometry of the measurement.

By using a slightly modified version of Eq. (30), a false target can be induced at a desired location by modifying the transmitted waveform to incorporate an incremental shift. The modification was necessary due to one-way (instead of two-way) propagation, as shown in Figure 6. In order to create an 'echo' for reference, two pulses were transmitted. The first pulse was unmodified (where α and τ_j are set to zero) for the 'echo'. The second pulse was modified using the corresponding values for τ_j and α to create the false target. The variables of the trajectory (V, R_0 and x_0) and the carrier frequency, were assumed to be known to the jammer. For the measurements, a Linear Frequency Modulated (LFM) or 'Chirp' waveform was used to created the bandwidth of 30MHz as listed in Table 2. This meant that

$$x(t) = e^{i\pi\gamma t^2} Rect\left(\frac{t}{\tau}\right) \tag{40}$$

where

$$Rect\left(\frac{t}{\tau}\right) = \begin{cases} 1, & 0 < t < \tau \\ 0, & \text{Elsewhere} \end{cases} \tag{41}$$

Using the derived jamming scheme, the first step was to create a false target at an additional cross-range only, without an additive range ($\tau_J = 0$). Figures 7 and 8 show that a target can be induced to have a cross-range position of 10m. The cross-range position of the antenna was 2.65m which meant that $\delta_x = 7.35$m to give the final cross-range position of 10m. These figures demonstrate the effectiveness of the jamming scheme to create a false target at the desired location in cross-range.

An additional downrange component can be added to the false target by delaying the transmitted pulse. In this case, the desired cross-range value was nominally 60m and downrange value was 35m. From Figure 6, the position of the transmit antenna (relative to the receive antenna) was 2.65m in cross-range and 4m in downrange. Therefore, to create a false target at 60m in cross-range and 35m in downrange, the values of δ_x and $\frac{2\tau_J}{c}$ were 57.35m and 31m, respectively. Figure 9 shows the cross-range (Doppler) profile of the false

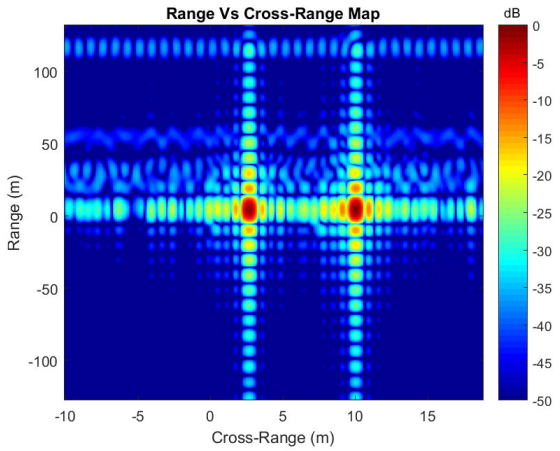

FIGURE 8. Range - cross-range map of 'Echo' and false target when $\tau_J = 0$ and $\delta_x = 7.35$m.

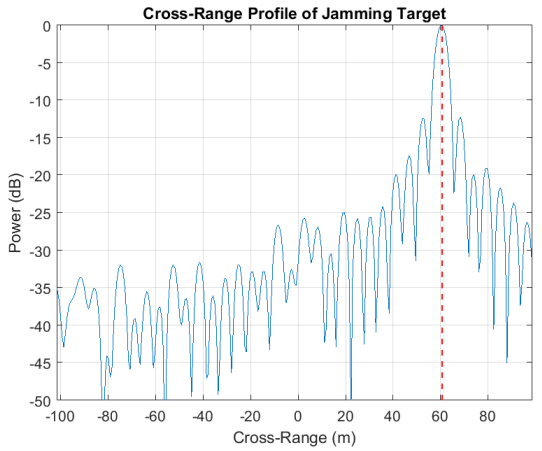

FIGURE 9. Cross-range profile of false target when $\frac{2\tau_J}{c} = 31$ and $\delta_x = 57.35$m.

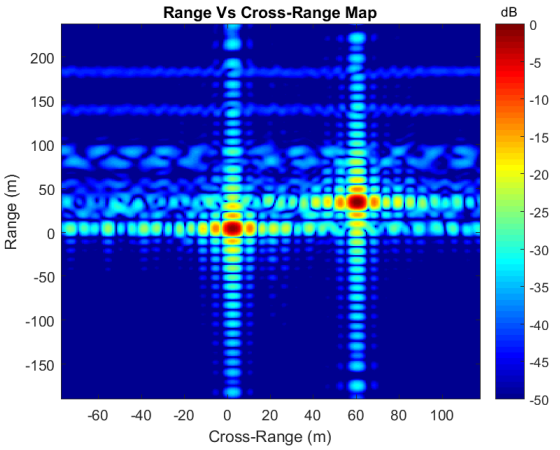

FIGURE 10. Range - cross-range map of 'Echo' and false target when $\frac{2\tau_J}{c} = 31$m and $\delta_x = 57.35$m.

target at 60m cross-range and Figure 10 shows a false target at 60m cross-range and 35m in downrange.

Following from Figure 4 and by using Eq. (34), Figure 11 shows how the cross-range position for the generated target

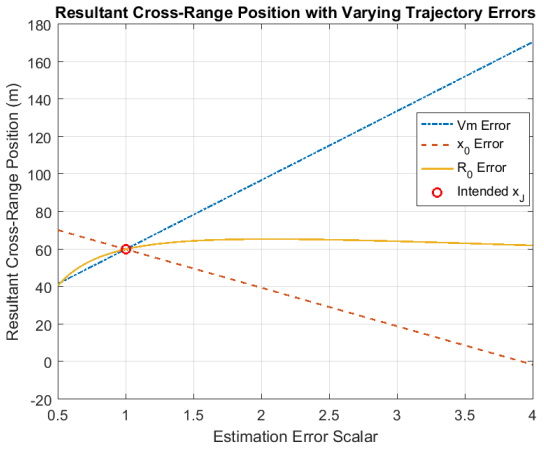

FIGURE 11. Resultant cross-range position for each error scalar.

FIGURE 12. Cross-range position of false target with erroneous initial seeker cross-range estimation.

TABLE 3. Error variables.

Error	Symbol	Scalar Value	$\hat{x}$ Prediction	$\hat{x}$ Result
Velocity	V_ϵ	2	96.85m	97.52m
Range	R_ϵ	2	65.42m	66.09m
Cross-Range	x_ϵ	4	-1.515m	-0.85m

will change with each error of velocity magnitude, cross-range and down-range. The figure was calculated with the intended false target position of 35m in downrange and 60m in cross-range. The Figure is used to demonstrate how the error scalars can be used to predict the cross-range position.

To verify Figure 11, several more measurements were taken and errors were systematically introduced as shown in Table 3. The cross-range prediction ($\hat{x}$) was calculated using Eq. (34). The table details the resultant cross-range position should the jamming equation include errors from one particular error per measurement. For example, the top line of the Table states that the velocity scalar, V_ϵ has a value of 2. This means that if the jammer uses the same variables as detailed in Table 2, every other variable was assumed to be correct, but the jammer modified the waveform to include a velocity of 120m/s and not 60m/s.

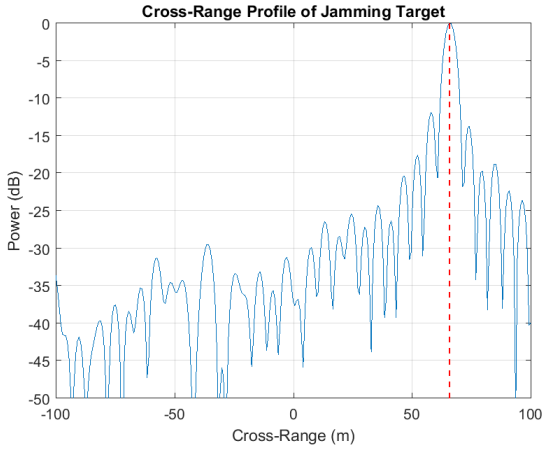

FIGURE 13. Cross-range position of false target with erroneous initial seeker downrange estimation.

FIGURE 14. Cross-range position of false target with erroneous initial seeker velocity estimation.

The cross-range (remapped Doppler) profiles for each of the measurements are shown in Figures 12, 13 and 14, respectively. For each of the plots, the intended cross-range position of the target (if there were no errors) was 60m. These three results show that the predictions in Figure 11 will hold when the scenario is scaled up to a more realistic scenario, shown in Figure 4.

V. CONCLUSION

A jamming technique to insert a false target at a desired location within the seeker image has been developed and tested with an experimental setup. We have shown that in order to place a false target in a desired location, the jammer only needs to apply a delay and a Doppler shift to the received signal. A further investigation should be undertaken using a DRFM in real-time to test the jamming scheme in a more realistic scenario.

The expected trajectories for the missile will generally be such that $R_0 \gg x_0$ which means the cross-range component of the trajectory will be small, relative to the downrange component. Therefore, errors in cross-range estimation yield smaller errors in the false target position than for downrange estimate errors. The largest source of error in the false target position is that of the velocity parameter. As a general result, the experimental and simulated results therefore show it would be better to concentrate resources on estimating the velocity rather than downrange or cross-range parameters of the incoming missile.

Future studies should be undertaken to assess how this could change for a different type of trajectory that a missile using DBS could take. The research should also be continued to assess the probability of the seeker accepting or rejecting the false targets generated using the described algorithm.

REFERENCES

[1] D. R. Wehner, *High-Resolution Radar*, 2nd ed. Norwood, MA, USA: Artech House, 1995.
[2] N. Stansfield, "A missile seeker and guidance method," MBDA UK, Stevenage, U.K., Tech. Rep., 2016, p. 10.
[3] K. H. Kim, S. G. Kim, and J. W. Yi, "Detection of ship targets near coastline by using Doppler beam sharpening technique," in *Proc. 3rd Int. Asia–Pacific Conf. Synth. Aperture Radar (APSAR)*, no. 1, 2011, pp. 774–777.
[4] A. Laribi, M. Hahn, J. Dickmann, and C. Waldschmidt, "Vertical Doppler beam sharpening goes self parking," in *Proc. IEEE Radar Conf. (RadarConf)*, Apr. 2018, pp. 383–388.
[5] L. Daniel, A. Stove, E. Hoare, D. Phippen, M. Cherniakov, B. Mulgrew, and M. Gashinova, "Application of Doppler beam sharpening for azimuth refinement in prospective low-THz automotive radars," *IET Radar, Sonar Navigat.*, vol. 12, no. 10, pp. 1121–1130, Oct. 2018.
[6] G. W. Stimson, H. H. Griffiths, C. Baker, and D. Adamy, *Stimson's Introduction to Airborne Radar*, 3rd ed. Rijeka, Croatia: SciTech, 2014.
[7] H. Paik, N. N. Sastry, and I. Santiprabha, "Effectiveness of noise jamming with White Gaussian noise and phase noise in amplitude comparison monopulse radar receivers," in *Proc. IEEE Int. Conf. Electron., Comput. Commun. Technol. (CONECCT)*, Jan. 2014, pp. 1–5.
[8] H. Paik, N. N. Sastry, and I. Santiprabha, "Effectiveness of repeat jamming using linear FM interference signal in monopulse receivers," *Procedia Comput. Sci.*, vol. 57, pp. 296–304, Jan. 2015.
[9] H. Paik, N. N. Sastry, and I. Santiprabha, "Estimation of break-lock in PLL synthesizers for monopulse radar applications: Experimental and simulation approach," *Int. J. Eng. Sci. Technol.*, vol. 19, no. 1, pp. 22–30, Mar. 2016.
[10] F. Neri, "Anti-monopulse jamming techniques," in *IEEE MTT-S Int. Microw. Symp. Dig.*, Nov. 2002, pp. 45–50.
[11] S.-Y. Liu, C.-X. Dong, J. Xu, G.-Q. Zhao, and Y.-T. Zhu, "Analysis of rotating cross-eye jamming," *IEEE Antennas Wireless Propag. Lett.*, vol. 14, pp. 939–942, Dec. 2015.
[12] L. Falk, "Cross-eye jamming of monopulse radar," in *Proc. Int. Waveform Diversity Design Conf.*, Jun. 2007, pp. 209–213.
[13] W. P. Plessis, "Practical implications of recent cross-eye jamming research," Council Sci. Ind. Res., Pretoria, South Africa, Tech. Rep., 2012, vol. 2.
[14] W. P. Du Plessis, J. W. Odendaal, and J. Joubert, "Extended analysis of retrodirective cross-eye jamming," *IEEE Trans. Antennas Propag.*, vol. 57, no. 9, pp. 2803–2806, Sep. 2009.
[15] W. P. Du Plessis, "Statistical skin-return results for retrodirective cross-eye jamming," *IEEE Trans. Aerosp. Electron. Syst.*, vol. 55, no. 5, pp. 2581–2591, Oct. 2019.
[16] A. De Martino, *Introduction to Modern EW Systems*, 2nd ed. Norwood, MA, USA: Artech House, 2018.
[17] Z. Shenghua, X. Dazhuan, J. Xueming, and H. Hua, "A study on active jamming to synthetic aperture radar," in *Proc. 3rd Int. Conf. Comput. Electromagn. Appl. (ICCEA)*, Jun. 2005, pp. 403–406.
[18] D. Da-Hai, X. F. Wu, W. Xue-Song, and X. Shun-Ping, "SAR active-decoys jamming based on DRFM," in *Proc. IET Int. Conf. Radar Syst.*, 2007, p. 43.
[19] R. S. Harness and M. C. Budge, "A study on SAR noise jamming and false target insertion," in *Proc. IEEE SOUTHEASTCON*, Mar. 2014, pp. 1–8.
[20] X. He, J. Zhu, J. Wang, D. Du, and B. Tang, "False target deceptive jamming for countering missile-borne SAR," in *Proc. IEEE 17th Int. Conf. Comput. Sci. Eng.*, Dec. 2014, pp. 1974–1978.

[21] Q. Sun, T. Shu, S. Zhou, B. Tang, and W. Yu, "A novel jamming signal generation method for deceptive SAR jammer," in *Proc. IEEE Radar Conf.*, May 2014, pp. 1174–1178.
[22] B. Lv, "Simulation study of noise convolution jamming countering to SAR," in *Proc. Int. Conf. Comput. Design Appl.*, Jun. 2010, pp. V4-130–V4-133.
[23] H. Hong-Xu, Z. Yi-Yu, J. Wen-Li, and H. Zhi-Tao, "A new time-delay echo jamming style to SAR," in *Proc. 2nd Int. Conf. Signal Process. Syst.*, Jul. 2010, pp. V3-14–V3-17.
[24] L. Huang, C. Dong, Z. Shen, and G. Zhao, "The influence of rebound jamming on SAR GMTI," *IEEE Geosci. Remote Sens. Lett.*, vol. 12, no. 2, pp. 399–403, Feb. 2015.
[25] W. Wang and J. Cai, "A technique for jamming bi- and multistatic SAR systems," *IEEE Geosci. Remote Sens. Lett.*, vol. 4, no. 1, pp. 80–82, Jan. 2007.
[26] X. Pan, D. Feng, Q. Fu, W. Wang, Y. Liu, and G. Wang, "On deception jamming for countering bistatic ISAR based on sub-Nyquist sampling," *IET Radar, Sonar Navigat.*, vol. 8, no. 3, pp. 173–179, Mar. 2014.
[27] W. Wang, X.-Y. Pan, Y.-C. Liu, D.-J. Feng, and Q.-X. Fu, "Sub-Nyquist sampling jamming against ISAR with compressive sensing," *IEEE Sensors J.*, vol. 14, no. 9, pp. 3131–3136, Sep. 2014.
[28] M. Rollason, D. Salmond, and M. Evans, "Parameter estimation for terminal guidance using a Doppler beam sharpening radar," in *Proc. AIAA Guid., Navigat., Control Conf. Exhib.* Reston, VA, USA: American Institute of Aeronautics and Astronautics, Aug. 2003, p. 5447.
[29] A. Farooq and D. J. N. Limebeer, "Optimal trajectory tracking for missiles with Doppler Beam Sharpening radars," in *Proc. Eur. Control Conf. (ECC)*, Jul. 2007, pp. 3985–3992.
[30] J. Hodgson and D. Lee, "Terminal guidance using a Doppler beam sharpening radar," in *Proc. AIAA Guid., Navigat., Control Conf. Exhibit.* Reston, VA, USA: American Institute of Aeronautics and Astronautics, Aug. 2003, p. 5796.
[31] G. Frazer, A. Balleri, and G. Jacob, "Simulations of repeat jamming against anti-ship missile seekers which use Doppler beam sharpening modes," in *Proc. Sensor Signal Process. Defence Conf. (SSPD)*, Dec. 2017, pp. 1–5.
[32] G. Frazer, A. Balleri, and G. S. Jacob, "Deception jamming against Doppler beam sharpening radars," in *Proc. IEEE Radar Conf. (RadarConf)*, Apr. 2019, pp. 1–6.
[33] H. L. Van Trees, *Detection, Estimation, and Modulation Theory, Part III*. New York, NY, USA: Wiley, 2001, p. 241.
[34] M. I. M. I. Skolnik, *Introduction to Radar System*, 3rd ed. New York, NY, USA: McGraw-Hill, 2001.
[35] C. A. Balanis, *Antenna Theory: Analysis and Design*. Hoboken, NJ, USA: Wiley, 2015.

GARETH FRAZER received the B.Eng. degree (Hons.) in avionics technology from Coventry University, Coventry, U.K., in 2014. He is currently pursuing the Ph.D. degree in radar electronic countermeasures with Cranfield University, Shrivenham, U.K. His research interests include radar design and countermeasure techniques against Doppler beam sharpening radars.

ALESSIO BALLERI received the Laurea degree *(summa cum laude)* (five legal years) from the University of Pisa, Pisa, Italy, in 2004, and the Ph.D. degree in electronic and electrical engineering from the University College London (UCL), London, U.K., in 2010. From February 2010 to March 2012, he was a Research Associate in radar systems with the Department of Electronic and Electrical Engineering, UCL. From June 2004 to December 2004, he was a Visiting Research Scholar with the Department of Electrical and Computer Engineering, University of Illinois at Chicago. He is currently a Reader in radar systems with Cranfield University, Shrivenham, U.K. His research interests include radar and sonar system design, biologically inspired radar and sonar systems, adaptive radar, radar and sonar target classification, target feature extraction, and modelling of radar clutter. He guest co-edited a special issue on "Biologically Inspired Radar and Sonar Systems" for the IET Radar, Sonar and Navigation in 2012 and a special issue on "Emerging Radar Techniques" for the *EURASIP Journal on Advances in Signal Processing*, in 2013. He was the Technical Program Committee Co-Chair for the IET International Radar Conference 2017 (Belfast, U.K.) and is the Technical Co-Chair of the 2020 IEEE International Radar Conference (Washington, DC, USA).

GEORGE JACOB received the B.Tech. degree (Hons.) in electrical engineering from IIT Kgp, India, in 1982, and the M.Sc. degree in digital communication systems from Loughborough University, U.K., in 1985. He joined the London South Bank University as a Researcher/Lecturer, from 1986 to 1990. He was also an Associate Lecturer with Open University, from 2002 to 2005. He joined MOD-UK, in 2005, and DSTL, in 2007. He is currently a Senior Scientist at DSTL. He holds two patents. His research interests include communications signal processing, radar signal processing, computational electromagnetics, and computational acoustics. He is a Charted Engineer with the IET and a Charted Scientist with the British Computer Society.